PARTICLE FILTER FOR SEQUENTIAL DETECTION AND TRACKING OF AN EXTENDED OBJECT IN CLUTTER

Branko Ristic and Jamie Sherrah

ISR Division, DSTO, Australia
email: {branko.ristic; jamie.sherrah}@dsto.defence.gov.au

ABSTRACT

The problem is joint detection and tracking of a non-point or extended moving object, characterised by multiple feature points which can result in detections. Due to imperfect detection, only some of the feature points are detected and in addition false alarms (or clutter) can also be present. Standard tracking techniques assume point objects, that is at most one detection per object, and hence are not adequate for this problem. The paper presents a theoretical solution in the form of the optimal Bayes filter, referred to as the Bernoulli filter for an extended object. The derivation follows the random set filtering framework introduced by Mahler. The filter is implemented approximately as a particle filter and subsequently tested using simulated data.

Index Terms— Tracking, extended object, random set theory, Bayes filtering

1. INTRODUCTION

Conventional tracking algorithms [1], historically developed for radar/sonar applications, assume that targets (moving objects) are points in the state space which result in at most one detection (measurement or observation) per target. This assumption is not appropriate for sensors, such as the high resolution radar or a video camera, where individual features (scattering or measurement generating points) of the target can be resolved and consequently the sensor can provide more than one detection per object. The problem of tracking extended objects has therefore attracted a lot of interest in the last decade, see [2, 3, 4, 5].

Among various approaches to extended target tracking, in this paper we are primarily interested in those based on the random set theory [6]. This theory has recently made a profound impact on the theoretical developments of sequential Bayesian estimation. As a result, the scope of applications of optimal nonlinear filtering has shifted from a single to multiple appearing/disappearing objects, from precise to imprecise and fuzzy measurements and measurement models.

Using the Poisson model of extended object detections [7], Mahler formulated the probability density hypothesis (PHD) filter for tracking multiple extended objects [8]. The cardinalised PHD (CPHD) filter for extended targets has been subsequently proposed in [9]. Both the PHD and CPHD filters for multiple extended object filtering are notoriously computationally intensive and perform poorly at a low probability of detection. A different approach was taken in [10]: the problem was formulated in the framework of doubly-stochastic point process theory, with analytic solution provided as the first order moment approximation. The filter in [10] provides sequential estimate of individual feature points but is limited to a single extended object which exists all the time.

In this paper we take yet another approach in the random set theoretical framework. We formulate the optimal Bayesian filter for joint detection and state estimation of an extended appearing/disappearing object in the presence of clutter. The solution is the Bernoulli filter (also known as JoTT filter) [6], [11], [12], [13] formulation for an extended object detection and tracking, which, as opposed to other mentioned approaches, is optimal. Its implementation, however, is based on the sequential Monte Carlo approximation, and the resulting algorithm will be referred to as the Bernoulli particle filter in the text. The main characteristic of the proposed Bernoulli filter is that it estimates jointly the probability of object existence and the spatial posterior probability density function (PDF) of the extended object. The probability of existence is important in determining the presence or absence of the object from the scene. The proposed Bernoulli filter does not estimate individual feature points and therefore is computationally tractable, as it will be demonstrated by numerical examples.

2. MATHEMATICAL MODELS

Consider an extended object whose characteristics of interest, such as position, heading, speed, shape and orientation parameters, are specified by the state vector $\mathbf{x}_k \in \mathcal{X}$, where k is the discrete-time index and $\mathcal{X}$ is the state space. The evolution of target state in time is assumed to be a Markov process with transition density $\pi(\mathbf{x}_k|\mathbf{x}_{k-1})$. In order to model the dynamics of object presence or absence from the surveillance volume of interest, we introduce a binary random variable $\epsilon_k \in \{0, 1\}$, referred to as the *target existence* (the adopted convention is that $\epsilon_k = 1$ means that target exists at time k).

The dynamics of ϵ_k is modelled by a two-state Markov chain with a transitional probability matrix (TPM) Π. The elements of the TPM are defined as $[\Pi]_{ij} = P\{\epsilon_{k+1} = j-1|\epsilon_k = i-1\}$ for $i, j \in \{1, 2\}$. We adopt a TPM as follows:

$$\Pi = \begin{bmatrix} (1-p_b) & p_b \\ (1-p_s) & p_s \end{bmatrix} \tag{1}$$

where $p_b := P\{\epsilon_{k+1} = 1|\epsilon_k = 0\}$ is the probability of target "birth"and $p_s := P\{\epsilon_{k+1} = 1|\epsilon_k = 1\}$ the probability of target "survival". These two probabilities together with the initial target existence probability $q_0 = P\{\epsilon_0 = 1\}$ are assumed known. Typically $q_0 = 0$, p_b is small and p_s is close to 1.

The extended object measurement model is adopted from [6, Sec. 12.7.1]. The assumption is that at time k, the object consists of L_k scattering (feature or measurement generating) points. Each of these points is specified by the state $\mathbf{y}_k^\ell \in \mathcal{Y}$, with $\ell = 1, \ldots, L_k$. The state space of scattering points $\mathcal{Y} \subset \mathcal{X}$, because it includes only characteristics such as position, heading and speed, but not the shape, size or orientation parameters. The probability of detection of a scattering point $\ell = 1, \ldots, L_k$ is assumed state independent and denoted by p_{D}^ℓ (the state dependent case can be easily handled, but is omitted here for clarity). Let $\mathbf{Z}_k = \{\mathbf{z}_1, \ldots, \mathbf{z}_m\}$ denote the set of detections or measurements, collected by the sensor at time k. The measurement space is denoted $\mathcal{Z}$. The set $\mathbf{Z}_k$ contains both the object generated measurements and false measurements (clutter). If a scattering point of an extended object in state $\mathbf{x}$ is detected and results in a measurement $\mathbf{z} \in \mathbf{Z}_k$, then its likelihood function is denoted by $g_k(\mathbf{z}|\mathbf{x})$. The false detections are assumed independent of the object state. Their count at time k is modelled by a Poisson distribution with mean λ. Their spatial distribution is assumed known and denoted by $c(\mathbf{z})$.

In order to write down the likelihood function of the extended object under the described assumptions it is convenient to introduce the concept of a random finite set (RFS) and its probability density function [6]. A RFS is a probabilistic representation of spatial point patterns that accounts for uncertainty in both the number of elements (points) in the set and the spatial locations of the points over the state space. A RFS Σ is therefore completely specified by a discrete distribution that characterises the cardinality of Σ and a joint spatial distribution of points in Σ conditional on cardinality. The probability density function (PDF) $f(\Sigma)$ of a RFS $\Sigma = \{s_1, \ldots, s_n\}$, $n \geq 0$, is integrated using the *set integral* [6].

The measurement set $\mathbf{Z}_k$ can clearly be modelled by a RFS: both its cardinality and the spatial distribution of measurement points in $\mathcal{Z}$ are random. Moreover, even the (extended) object of interest can be modelled by a random finite set $\mathbf{X}_k$, which can be either empty (when target is absent, $\mathbf{X}_k = \emptyset$) or contain a single element (when target is present, $\mathbf{X}_k = \{\mathbf{x}_k\}$). This type of a RFS, which can be either empty or a singleton, is referred to as the Bernoulli RFS [6].

The likelihood function of the extended object has been specified in [6, Sec. 12.7.1]. This expression can be simplified due to the lack of knowledge about individual scattering points. Suppose for all of them the probability of detection is $p_{\text{D}}^\ell = p_{\text{D}}$, $\ell = 1, \ldots, L_k$. Then the likelihood function is given by:

$$\varphi_k(\mathbf{Z}|\{\mathbf{x}\}) = \kappa(\mathbf{Z}) \Big\{ (1-p_{\text{D}})^{L_k} + \sum_{\Omega \in \mathcal{P}_{1:L_k}(\mathbf{Z})} p_{\text{D}}^{|\Omega|} (1-p_{\text{D}})^{L_k - |\Omega|} \prod_{\mathbf{z} \in \Omega} \frac{g_k(\mathbf{z}|\mathbf{x})}{\lambda\, c(\mathbf{z})} \Big\} \tag{2}$$

where $\kappa(\mathbf{Z}) = \varphi_k(\mathbf{Z}|\emptyset) = e^{-\lambda} \lambda^{|\mathbf{Z}|} \prod_{\mathbf{z} \in \mathbf{Z}} c(\mathbf{z})$ is the PDF of the Poisson RFS of false detections, and $\mathcal{P}_{1:L}(\mathbf{Z})$ is the set of all subsets of the measurement set $\mathbf{Z}$, with cardinality equal to $1, 2, \ldots, L$.

The potential difficulty with expression (2) for the likelihood function of an extended object is that L_k is unknown and not included it in the state vector $\mathbf{x}_k$. We will show later that L_k can be estimated impact in Sec.5.

3. BERNOULLI FILTER EQUATIONS

Suppose the posterior PDF of extended object at time k is available and denoted $f_{k|k}(\mathbf{X}|\mathbf{Z}_{1:k})$, where

$$\mathbf{Z}_{1:k} \equiv \mathbf{Z}_1, \mathbf{Z}_2, \ldots, \mathbf{Z}_k$$

is the sequence of measurement sets collected up to time k. The Bayes filter propagates the posterior PDF sequentially over time, as the new sets of measurements become available. The extended object state $\mathbf{X}_k$ can be modelled by a Bernoulli RFS, for which the posterior PDF has the form [6]:

$$f_{k|k}(\mathbf{X}|\mathbf{Z}_{1:k}) = \begin{cases} 1 - q_{k|k} & \text{if } \mathbf{X} = \emptyset \\ q_{k|k} \cdot s_{k|k}(\mathbf{x}) & \text{if } \mathbf{X} = \{\mathbf{x}\} \\ 0 & \text{if } |\mathbf{X}| > 1 \end{cases} \tag{3}$$

where

- $q_{k|k} = P\{\epsilon_k = 1|\mathbf{Z}_{1:k}\}$ is the posterior probability of object existence;
- $s_{k|k}(\mathbf{x}) = p_k(\mathbf{x}|\mathbf{Z}_{1:k})$ is the posterior PDF over the state space $\mathcal{X}$ (the spatial posterior PDF).

The Bernoulli filter is completely specified by the pair $\Big(q_{k|k}, s_{k|k}(\mathbf{x})\Big)$ and next we formulate the prediction and update equations for these two quantities.

Since the state vector does not include individual scattering points, the prediction equations are identical to those of the standard Bernoulli filter. According to [6, Sec.14.7], the prediction from time $k-1$ to k is carried out as follows:

$$q_{k|k-1} = p_b \cdot (1 - q_{k-1|k-1}) + p_s \cdot q_{k-1|k-1} \tag{4}$$

$$s_{k|k-1}(\mathbf{x}) = \frac{p_b \cdot (1-q_{k-1|k-1}) \int \pi_{k|k-1}(\mathbf{x}|\mathbf{x}')\, b_{k-1}(\mathbf{x}')\, d\mathbf{x}'}{q_{k|k-1}} + \frac{p_s\, q_{k-1|k-1} \int \pi_{k|k-1}(\mathbf{x}|\mathbf{x}')\, s_{k-1|k-1}(\mathbf{x}')\, d\mathbf{x}'}{q_{k|k-1}} \quad (5)$$

The density $b_{k-1}(\mathbf{x})$ in (5) represents the spatial distribution of "target birth". It is typically implemented in an adaptive manner using prior knowledge and the measurement set from the previous scan (i.e. $\mathbf{Z}_{k-1}$).

We next present the update equations of the Bernoulli filter for an extended object. The derivation is omitted due to the lack of space. The update equation for the probability of existence is given by:

$$q_{k|k} = \frac{1-\Delta_k}{1-\Delta_k\, q_{k|k-1}}\, q_{k|k-1} \quad (6)$$

where

$$\Delta_k = 1-(1-p_{\text{D}})^{L_k} - \sum_{\Omega\in\mathcal{P}_{1:L_k}(\mathbf{Z}_k)} \frac{p_{\text{D}}^{|\Omega|}}{(1-p_{\text{D}})^{|\Omega|-L_k}} \frac{\int \prod_{\mathbf{z}\in\Omega} g(\mathbf{z}|\mathbf{x})\cdot s_{k|k-1}(\mathbf{x})\, d\mathbf{x}}{\prod_{\mathbf{z}\in\Omega}\lambda\, c(\mathbf{z})}. \quad (7)$$

The update equation for the spatial posterior PDF is given by:

$$s_{k|k}(\mathbf{x}) = \left[\frac{(1-p_{\text{D}})^{L_k}}{1-\Delta_k} + \frac{\sum_{\Omega\in\mathcal{P}_{1:L_k}(\mathbf{Z}_k)} \frac{p_{\text{D}}^{|\Omega|}}{(1-p_{\text{D}})^{|\Omega|-L_k}} \prod_{\mathbf{z}\in\Omega} \frac{g_k(\mathbf{z}|\mathbf{x})}{\lambda\, c(\mathbf{z})}}{1-\Delta_k}\right] s_{k|k-1}(\mathbf{x}). \quad (8)$$

It can be easily verified that by setting $L_k = 1$, eqs. (7) and (8) simplify to

$$\Delta_k = p_{\text{D}}\left(1 - \sum_{\mathbf{z}\in\mathbf{Z}_k} \frac{\int g(\mathbf{z}|\mathbf{x})\cdot s_{k|k-1}(\mathbf{x})\, d\mathbf{x}}{\lambda\, c(\mathbf{z})}\right) \quad (9)$$

and

$$s_{k+1|k+1}(\mathbf{x}) = \frac{1-p_D+p_D \sum_{z\in Z_{k+1}} \frac{g_{k+1}(z|\mathbf{x})}{\lambda c(z)}}{1-\Delta_{k+1}}\, s_{k+1|k}(\mathbf{x}) \quad (10)$$

respectively. Equations (9) and (10) are well known for the standard (point-target) Bernoulli filter [6, Sec.14.7.4],[13].

4. IMPLEMENTATION

The numerical implementation of the proposed Bernoulli filter for joint detection/tracking of an extended object is based on approximations. The spatial PDF $s_{k|k}(\mathbf{x})$ is approximated by a set of N weighted random samples (i.e. particles) $\{w^i_{k|k}, \mathbf{x}^i_{k|k}\}_{i=1}^N$, where $\mathbf{x}^i_{k|k}$ is the state of particle i and $w^i_{k|k}$ is its corresponding weight. The weights are normalised, i.e. $\sum_{i=1}^N w^i_{k|k} = 1$. The approximation of $s_{k|k}(\mathbf{x})$ can then be written as

$$s_{k|k}(\mathbf{x}) \approx \sum_{i=1}^{N} w^i_{k|k}\, \delta_{\mathbf{x}^i_{k|k}}(\mathbf{x}) \quad (11)$$

where $\delta_{\mathbf{a}}(\mathbf{x})$ is the Dirac delta function concentrated at $\mathbf{a}$. The prediction and update of both $q_{k|k}$ and $s_{k|k}(\mathbf{x})$ are then implemented in a similar manner as in the standard (point target) Bernoulli particle filter, which is described in detail in [13]. The main difference is that: (1) the so called "birth" particles are formed based on every subset $\Omega \in \mathcal{P}_{1:L_{k-1}}(\mathbf{Z}_{k-1})$; (2) the weights of particles are updated according to (8) as:

$$w^i_{k|k} \propto \left[(1-p_{\text{D}})^{L_k} + \sum_{\Omega\in\mathcal{P}_{1:L_k}(\mathbf{Z}_k)} \frac{p_{\text{D}}^{|\Omega|}}{(1-p_{\text{D}})^{|\Omega|-L_k}} \prod_{\mathbf{z}\in\Omega} \frac{g_k(\mathbf{z}|\mathbf{x})}{\lambda\, c(\mathbf{z})}\right] \cdot w^i_{k|k-1} \quad (12)$$

After normalisation of weights, the particles are resampled N times to obtain a new set of equally weighted particles $\{\frac{1}{N}, \mathbf{x}^i_{k|k}\}_{i=1}^N$ which approximate $s_{k|k}(\mathbf{x})$.

Since L_k is unknown and not included it in the state vector $\mathbf{x}_k$, it is estimated as follows:

$$\widehat{L}_k = \min\left\{\left[\frac{|\mathbf{Z}_k|-\lambda}{p_{\text{D}}}\right], L^*\right\} \quad (13)$$

where $[\cdot]$ denotes for the nearest integer operation and parameter $L^* \in \mathbb{N}$ is adopted as a trade-off between the computational speed and accuracy. In general, the estimate $\widehat{L}_k$ will differ to some degree from the true value of L_k. However, we will see in the next section that a small error in estimation of L_k, is not critical because the relative ranking of the particle weights is almost unaffected by this error. Since the weights are normalised in the particle filter, only their ratio is important for survival in the resampling step.

The last approximation involves *gating* of measurements, that is the selection of a subset $\mathbf{Z}^*_k \subseteq \mathbf{Z}_k$ which has a reasonable chance of being due to the target. A measurement $\mathbf{z} \in \mathbf{Z}_k$ will be included in $\mathbf{Z}^*_k$ if $\sum_i\{g_k(\mathbf{z}|\mathbf{x}^i_{k|k-1})\} > \eta$, where $\eta \geq 0$ is a user specified threshold. The update step of the Bernoulli filter is in practice carried out using $\mathbf{Z}^*_k$, rather than $\mathbf{Z}_k$, in order to speed up the computation.

5. SIMULATION RESULTS

Consider a two-dimensional surveillance area in the Cartesian coordinates, specified by the lower-left corner $(0,0)$ and upper-right corner $(500,300)$. The extended target is of a Gaussian shape, specified by the mean (centroid) $\boldsymbol{\mu} = [x,y]^\intercal$,

its velocity vector $\mathbf{v} = [\dot{x}, \dot{y}]^\intercal$ and the ellipsoidal shape defined by parameters $\boldsymbol{\sigma} = [a, b, c]^\intercal$ which define the elements of the corresponding covariance matrix (a and b are diagonal elements). Hence the state vector consists of 7 components: $\mathbf{x} = [\boldsymbol{\mu}^\intercal \ \mathbf{v}^\intercal \ \boldsymbol{\sigma}^\intercal]^\intercal$. The target in state $\boldsymbol{\mu} = [180, \ 0]^\intercal$, $\mathbf{v} = [4, \ 4]^\intercal$ and $\boldsymbol{\sigma} = [60, \ 30, \ -5]^\intercal$ enters the surveillance area at $k = 5$ and leaves the area at $k = 72$. Its dynamics is described by the transitional density $\pi(\mathbf{x}|\mathbf{x}') = \mathcal{N}(\mathbf{x}; \mathbf{F}\mathbf{x}', \mathbf{Q})$, where $\mathbf{F}$ and $\mathbf{Q}$ are selected so that the centroid of the target travels with the nearly constant velocity [14]. The shape parameter vector is modelled by a random walk [14]. Fig.1.(c) shows a typical trajectory of the target centroid. The true number of scattering points L_k initially is 5 and then drop to 4. The probability of scattering point detection is set to $p_{\text{D}} = 0.6$, while the likelihood $g_k(\mathbf{z}|\mathbf{x}) = \mathcal{N}(\mathbf{z}; \boldsymbol{\mu}, \mathbf{S})$, where $\mathbf{S} = \begin{bmatrix} a & c \\ c & b \end{bmatrix}$. The false detections are uniformly distributed over the surveillance area with average count $\lambda = 5$.

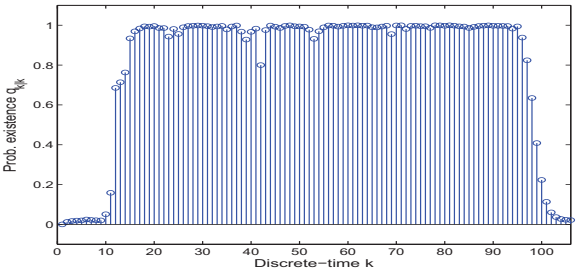

(a)

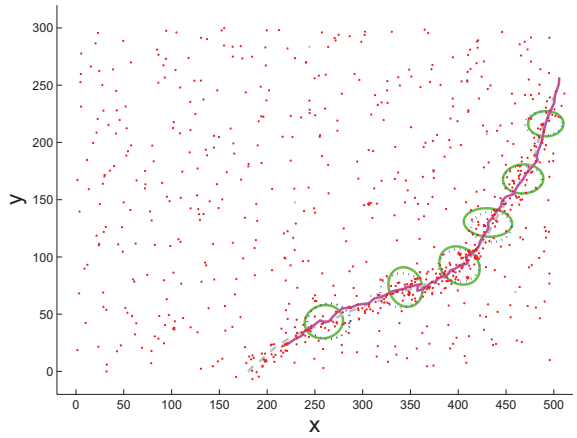

(b)

Fig. 1. A single run of the algorithm: (a) Posterior probability of existence $q_{k|k}$; (b) All detections, true (dashed line) and estimated (solid line) centroid trajectories; overlayed target shapes at $k = 20, 35, 55, 70, 80, 90$: true (dashed line) and estimated (solid line)

The results of a single run of the proposed Bernoulli particle filter (BPF) are shown in Fig.1. The BPF was implemented using $N_b = 100$ and $N = 5000$ particles, with the gating threshold $\eta = 100$ and $L^* = 7$. The probability $q_{k|k}$ in Fig.1.(a) determines with a small delay the presence of the object at about $k = 10$. It reliably stays at a very high value, almost equal to 1, until, again with a small delay, determines the that the objects has disappeared at about $k = 75$. The true and estimated trajectories of the target centroid are shown in Fig.1.(b). The estimates of the extended target are shown in Fig.1.(c) at $k = 20, 31, 42$ and 53. We notice a remarkable accuracy in estimating both the centroid and the size/orientation of the object. As we have anticipated in Sec.4, the error in the estimation of L_k does not appear to have a significant effect on the performance of the Bernoulli filter.

Next we analyse the error performance of the BPF using the optimal subpattern (OSPA) error [15]. The OSPA error is a proper metric between two sets of objects (i.e. the ground truth versus the estimate from the BPF) which penalises both the cardinality error (e.g. target present but not detected) and the error in the state space.

Suppose at time k the true object state is $\mathbf{X}_k$, while the estimated state is $\widehat{\mathbf{X}}_k$. Since the sets $\mathbf{X}_k$ and $\widehat{\mathbf{X}}_k$ can be either empty or singletons $\mathbf{X}_k = \{\mathbf{x}_k\}$ and $\widehat{\mathbf{X}}_k = \{\hat{\mathbf{x}}_k\}$, the definition of OSPA error from [15] simplifies to:

$$D(\mathbf{X}_k, \widehat{\mathbf{X}}_k) = \begin{cases} \min\{c, d(\mathbf{x}_k, \hat{\mathbf{x}}_k)\} & \mathbf{X}_k{=}\{\mathbf{x}_k\}, \widehat{\mathbf{X}}_k{=}\{\hat{\mathbf{x}}_k\} \\ c & |\mathbf{X}| \neq |\widehat{\mathbf{X}}_k| \\ 0 & \mathbf{X}_k = \widehat{\mathbf{X}}_k = \emptyset \end{cases} \tag{14}$$

where c is referred to as the cut-off parameter and $d(\mathbf{x}_k, \hat{\mathbf{x}}_k)$ is the base distance defined over $\mathcal{X}$. We consider two cases of OSPA error. In the first case, the base distance is defined as the Euclidian distance between the location of the true object centroid $\boldsymbol{\mu}_k$ and its estimate $\widehat{\boldsymbol{\mu}}_k$: $d_1(\mathbf{x}_k, \hat{\mathbf{x}}_k) = \| \boldsymbol{\mu}_k - \widehat{\boldsymbol{\mu}}_k \|$. This is referred to as the centroid localisation OSPA error, and its cut-off parameter is adopted as $c_1 = 10$. In the second case, the base distance is defined as the Euclidian distance between the shape/size parameters: $\boldsymbol{\sigma}_k$ (true) and $\widehat{\boldsymbol{\sigma}}_k$ (estimate): $d_2(\mathbf{x}_k, \hat{\mathbf{x}}_k) = \| \boldsymbol{\sigma}_k - \widehat{\boldsymbol{\sigma}}_k \|$. This is referred to as shape/size OSPA error and its cut-off parameter is adopted as $c_2 = 60$.

The two OSPA errors were averaged over 100 independent Monte Carlo runs and shown in Fig.2. The true object trajectory and shape/size was created with zero process noise (i.e. identical in each run), with the target present from $k = 5$ to $k = 78$. The results are computed for different values of L^*, that is $L^* = 1, 3, 5, 7$.

According to Fig.2, initially, in the absence of the target, the OSPA errors are zero. Then at $k = 5$, when the target appears, both the localisation and size/shape mean OSPA errors jump to the their respective cut-off values, due to a delay in track formation. Subsequently both OSPA errors reduce as the base distance component becomes the dominant source of error. The errors during this interval are reduced due to the BPF convergence. Then at time $k = 78$, the errors jump back

to their respective cut-off values, as a result of a delay in track termination. Eventually from $k = 88$ onwards both OSPA errors are zero again.

Regarding the the centroid localisation mean OSPA error in Fig.2.(a), one can observe that the choice of $L^* > 0$ does not seem to make a difference. This is a remarkable result, because the BPF at $L^* = 1$ reduces to the standard point-target BPF, characterised by a linear computational complexity with the number of measurements. Based on Fig.2.(a) we conclude that if one is interested only in the extended object centroid estimate, then it is adequate to use the standard point-target BPF (i.e. $L^* = 1$).

The shape/size mean OSPA error in Fig.2.(b), however, reveals that the choice of $L^* > 0$ can play a role in the estimation of object shape/size parameters. It appears that adopting $L^* = 3, 5, 7$ the BPF produces similarly accurate estimates of size/shape parameters. The size/shape estimates obtained using $L^* = 1$, however, were significantly less inaccurate.

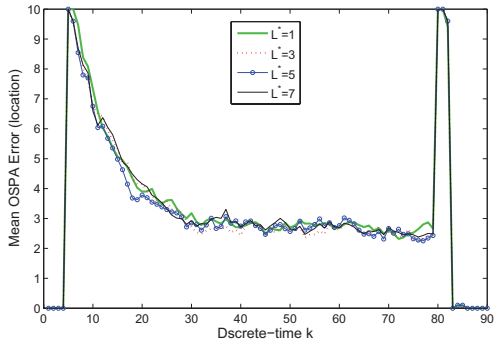

(a)

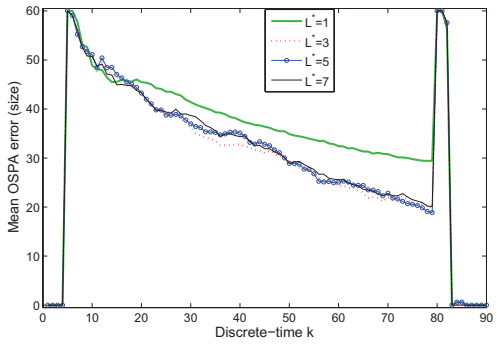

(b)

Fig. 2. Mean OSPA error using $L^* = 1, 3, 5, 7$: (a) object centroid localisation (b) object size/shape

6. CONCLUSIONS

The paper formulated the optimal Bayes filter for joint detection and tracking of an extended object in the presence of false detections. The implemented filter, referred to as the Bernoulli particle filter, is an approximation based on the sequential Monte Carlo method. The numerical analysis indicates that the BPF is accurate in both object centroid and size/shape estimation. If one is concerned only with centroid estimation, it is adequate to use the standard (point-object) BPF.

The BPF has been applied to tracking objects using corner detections in a video sequence, but the results are not included here due to the limited space.

Future work will formulate a multi-object version of this algorithm in the form of a multi-Bernoulli tracker for extended targets. This will be carried out by inclusion of a suitable data association technique as discussed in [16].

7. REFERENCES

[1] S. Blackman and R. Popoli. *Design and Analysis of Modern Tracking Systems*. Artech House, 1999.

[2] J. Vermaak, N. Ikoma, and S. Godsill. A sequential Monte Carlo framework for extended object tracking. *IEE Proc. Radar, Sonar and Navig.*, 152(5):353–363, 2005.

[3] K. Gilholm and D. Salmond. Spatial distribution model for tracking extended objects. *IEE Proc. Radar, Sonar Navig.*, 152(5):364–371, 2005.

[4] J. W. Koch. Bayesian approach to extended object and cluster tracking using random matrices. *IEEE Trans Aerospace and Electronic Systems*, 44(3):1042–1059, 2008.

[5] In *Proc. Int. Conf. Information Fusion*, Chicago, USA, July 2011. Special Session: Extended Object and group target tracking.

[6] R. Mahler. *Statistical Multisource Multitarget Information Fusion*. Artech House, 2007.

[7] K. Gilholm, S. Godsill, S. Maskell, and D. Salmond. Poisson models for extended target and group tracking. In *Proc. SPIE*, volume 5913, 2005.

[8] R. Mahler. PHD filters for nonstandard targets I: Extended targets. In *Proc. 12th Int. Conf. Information Fusion*, Seattle, USA, July 2009.

[9] U. Orguner, C. Lundquist, and Karl Granström. Extended target tracking with a cardinalized probability hypothesis density filter. In *Proc. 14th Int. Conf. Information Fusion*, Chicago, USA, July 2011.

[10] A. Swain and D. Clark. The single-group PHD filter: an analytic solution. In *Proc. 14th Int. Conf. Information Fusion*, Chicago, USA, July 2011.

[11] B.-T. Vo, C.-M. See, N. Ma, and W.-T. Ng. Multi-sensor joint detection and tracking with the Bernoulli filter. *IEEE Trans. Aerospace and Electronic Systems*, 2012. (To appear).

[12] B.-T. Vo, D. Clark, B.-N. Vo, and B. Ristic. Bernoulli forward-backward smoothing for joint target detection and tracking. *IEEE Trans Signal Processing*, 59(9):4473–4477, Sept. 2011.

[13] B. Ristic and S. Arulampalam. Bernoulli particle filter with observer control for bearings only tracking in clutter. *IEEE Trans. Aerospace & Electronic Systems*, 2012. (To appear).

[14] Y. Bar-Shalom, X. R. Li, and T. Kirubarajan. *Estimation with Applications to Tracking and Navigation*. John Wiley & Sons, 2001.

[15] D. Schuhmacher, B.-T. Vo, and B.-N. Vo. A consistent metric for performance evaluation of multi-object filters. *IEEE Trans. Signal Processing*, 56(8):3447–3457, Aug. 2008.

[16] J. L. Williams. Experiments with graphical model implementations of multiple target multiple Bernoulli filters. In *Proc. 7th Int. Conf Intelligent sensors, Sensor Networks and Information Processing*, pages 532–537, Adelaide, Australia, Dec. 2011.